IOP Publishing Journal of Physics D: Applied Physics
J. Phys. D: Appl. Phys. **40** (2007) 2045–2054 doi:10.1088/0022-3727/40/7/029

Power dissipation analysis in N_2O RF discharges using Monte Carlo modelling

G Younis, B Despax, M Yousfi and H Caquineau

Université Paul Sabatier, Laboratoire Plasma et Conversion d'Energie, UMR CNRS 5213,118 Route de Narbonne, 31 062 Toulouse, France

E-mail: georges.younis@insa-toulouse.fr

Received 6 October 2006, in final form 14 January 2007
Published 16 March 2007
Online at stacks.iop.org/JPhysD/40/2045

Abstract

In this paper, a microscopic approach for the calculation of partial and total power dissipation from energy losses by collisions is considered and applied in the case of N_2O low pressure RF discharges. This approach is based on a Monte Carlo technique in a particle model permitting sampling of the energy deposited by different inelastic electron–N_2O collisions. The calculated power densities presented in this paper are in good agreement with the experimental results and those obtained by the classical macroscopic formula based on spatio-temporal integration of the product of current density and electrical field. This microscopic approach presents, however, a major advantage in comparison with the classical method (which only offers the possibility to calculate the global power dissipation) by making possible the calculation of all the power density terms, thereby permitting one to examine the relative contribution of each collision process in the power dissipation. Its application to N_2O electronegative discharges, at 503 K gas temperature, several RF voltages and two different gas pressures shows how the power is dissipated through electron–gas processes. The power density variation is found to be proportional to the electron density variation brought about by the changes in attachment (i.e. $e + N_2O \rightarrow N_2 + O^-$), detachment (i.e. $NO^- + N_2O \rightarrow NO + N_2O + e$) and ionization (i.e. $e + N_2O \rightarrow N_2O^+ + 2e$) processes. The role of each of these processes is fully studied with our particle model in order to explain the dissipated power variation.

1. Introduction

Cold plasma processes due to low operating temperatures are currently unavoidable techniques in the microelectronics industry to deposit or etch layers while preserving the reliability of thermo-sensitive components [1]. More particularly, SiH_4 (silane)/N_2O (nitrous oxide) discharges with a very small amount of SiH_4 are widely used to deposit silicon oxide layers [2], which are very useful in the microelectronic industry [3]. In this kind of plasma process, the understanding and the control of the discharge are crucial for the optimization (homogeneity, mass density, etc) of the SiO_2 thin films. Such an optimization of the deposit needs, in fact, a good knowledge of the electric, energetic, hydrodynamic and mass transfer behaviour of the discharge. Preliminary hydrodynamic and electric modelling studies of pure N_2O [4] and N_2O/SiH_4 [5] discharges have already been undertaken. Although these papers demonstrate the main role of the attachment–detachment processes in the discharge sustaining, they do not study the role and the weight of the various processes responsible for the energy and power dissipation in the discharge.

The present work is devoted to a detailed study of the electrical and energetic aspects of N_2O RF discharges at different applied voltages and gas pressures. We thus study and analyse the charged particle energy and density variations as well as the roles of elastic and inelastic electron–N_2O collisions in the power dissipation.

A specific microscopic approach to calculate the partial and the total dissipated power density from the energy

deposited by the electrons–gas processes is proposed in the case of a N_2O low pressure RF discharge. This approach had already been used to study the penetration of energetic beams in gas for microdosimetric applications [6] and in matter for composite applications [7], in order to estimate the gas or matter stopping power.

Also, some authors in the literature used a similar approach in dc [8] and RF [9–11] discharges by resolving the Boltzmann equation with the help of fluid, hybrid and other models, often presuming the electron distribution function as maxwellian. The originality of our work resides in the fact that we calculated the collisional term of the energy conservation equation corresponding to the second moment of the Boltzmann equation using a particle model, without the need to resolve this equation or to presume a maxwellian distribution for the electrons.

It is also important to mention the works of Kawamura and Ingold [12] which study, using a particle model in the positive column of an argon glow discharge, the power balance between the Joule heating and the total losses of energy by collisions.

In addition to the classical method which uses a macroscopic law based on the spatio-temporal integration of the product of the current density and the electric field ($\vec{J} \cdot \vec{E}$) (see [13]), the present approach permits the determination of the energy deposited by collisions through the different processes involved in the discharge from the microscopic data (collision frequency, electronic density, etc).

In order to validate our calculation results, experimental measurements were carried out in the reactor described in section 2 hereafter. The discharge model is detailed in section 3 with a particular emphasis on the present approach for the determination of the power density dissipation from energy losses. Section 4 first compares the results of the proposed calculation approach with the classical one, followed by a discussion and analysis of the results with a special emphasis on the weight and role of the different collision processes in our N_2O discharges. The charged particle density and more particularly the electron density directly responsible for the power dissipation are analysed, explaining thereafter the different power dissipation behaviours at 0.5 and 1 Torr.

2. Overview of the experimental set up

Figure 1 shows a simplified view of the experimental RF reactor used in this study. It consists of a stainless steel plasma box divided into two symmetrical parts by a RF electrode.

In such a configuration, two symmetrical plasma zones are created between the excited electrode and the grounded walls. Gases are fed on both sides, at the top of the plasma box, through two narrow slits (0.3 mm × 250 mm). These gases are pumped out through two identical slits located at the bottom of the plasma box active zone, after flowing through the two plasma zones. The 13.56 MHz RF (25.6 × 25.6 cm^2) electrode is capacitively coupled to a RF generator by means of a LC matching box (figure 2). The inter-electrode distance is 3.95 cm. The RF voltage applied to the RF power driven electrode is measured using an oscilloscope (Tektronics TDS 410) via a high impedance Tek P5100 probe. Special

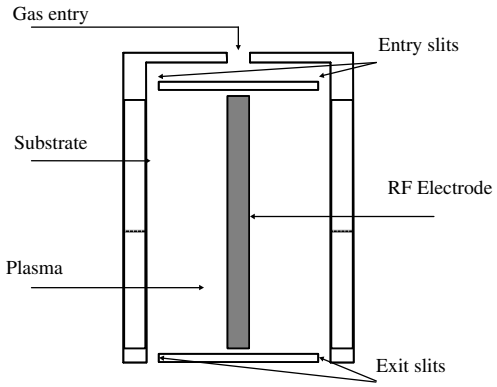

Figure 1. Simplified presentation of the RF reactor.

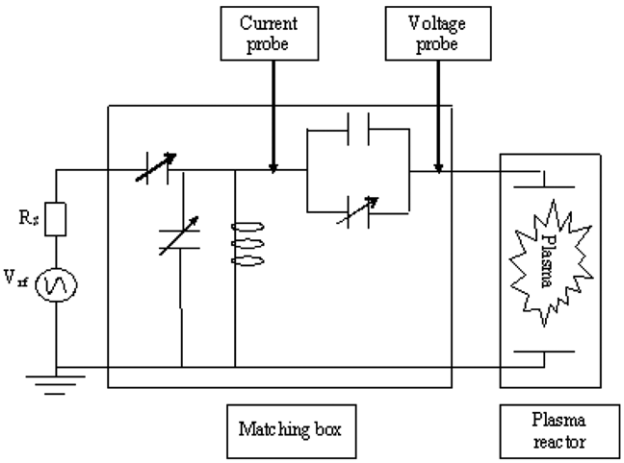

Figure 2. Matching box connecting the plasma discharge to the power supply.

attention was paid to make the measurements as close as possible to the real voltage applied to the electrode in order to avoid signal perturbations due to RF manipulations. The RF voltage probe measurement was carried out between the blocking capacitor (500 pF $\leqslant C_b \leqslant$ 1500 pF) of the matching box and the RF electrode. The electrode voltage $V(t)$ can be written $V(t) = V_{RF} \cos \omega t + V_{dc}$, where V_{RF} is the amplitude of RF voltage ($V_{RF} = V_{pp}/2$) and V_{dc} the direct current voltage. The voltage measurement did not bring out significant V_{dc} and so the RF discharge was considered as symmetrical in the following.

The real power injected was then estimated using a classical subtractive method [14]. Then, the power density was obtained by dividing the power by the mean electrode area covered by the plasma zones.

More details about this reactor can be found elsewhere [4]. As mentioned above, our modelling results are validated by experimental measurements such as the dissipated power.

3. Discharge particle model

3.1. General description

A powerful particle model already described elsewhere (see [4, 5]) is optimized and adapted in the present work for the electric and energetic study of the N_2O low pressure

Table 1. Electron and ion–gas interactions considered in this work with the corresponding references for the collision cross sections.

Electron–gas interactions		
$e + N_2O \rightarrow e + N_2O$	Elastic collision	[22]
$e + N_2O \rightarrow N_2 + O + e$	Dissociation	[22]
$e + N_2O \rightarrow NO + N + e$	Dissociation	[5]
$e + N_2O \rightarrow N_2O^* + e$	Electronic excitation	[5, 22]
$e + N_2O \rightarrow N_2^* + O + e$	Dissociative excitation	[5]
$e + N_2O \rightarrow N_2(A\ ^3\Sigma_u^+) + O(^3P) + e$	Dissociative excitation	[23]
$e + N_2O \rightarrow N_2 + O^* + e$	Dissociative excitation	[5, 22]
$e + N_2O \rightarrow N_2(X\ ^1\Sigma_g^+) + O(^1S) + e$	Dissociative excitation	[24]
$e + N_2O \rightarrow N_2O(1 \leqslant \nu \leqslant 3) + e$	Vibrational excitation	[22]
$e + N_2O \rightarrow O^-(^2P) + N_2(X\ ^1\Sigma_g^+)$	Attachment	[16, 25]
$e + N_2O \rightarrow N_2O^+ + 2e$	Ionization	[26]
Ion–neutral interactions		
$O^- + N_2O \rightarrow O^- + N_2O$	Elastic collision	[16]
$O^- + N_2O \rightarrow NO^- + NO$	O^- conversion into NO^-	[27]
$O^- + N_2O \rightarrow O_2^- + N_2$	O^- conversion into O_2^-	[27]
$NO^- + N_2O \rightarrow NO^- + N_2O$	Elastic collision	[16]
$NO^- + N_2O \rightarrow N_2O^- + NO$	Charge transfer	[27]
$NO^- + N_2O \rightarrow N_2O + NO + e$	Detachment	[16]
$N_2O^+ + N_2O \rightarrow N_2O^+ + N_2O$	Elastic collision	[5]
$N_2O^+ + N_2O \rightarrow N_2O + N_2O^+$	Charge transfer	[5]

RF discharges. The particle model considers the charged particles as a set of pseudo-particles undergoing collisions with neutral N_2O in the framework of weakly ionized gas approximation. The electron–molecule and ion–molecule processes are simulated with a Monte Carlo technique coupled to the Poisson equation. The Monte Carlo method is used for the collision treatment and the spatio-temporal characterization of every particle motion under the action of the electric field. The latter is calculated using the Poisson equation.

Generally, the main disadvantage of the usual particle models or PIC/MCC models is the important computing time. In addition to the optimization technique already known, i.e. the null collision method, different time steps for electron and ions, smoothing of particle densities before field calculation, etc, the particle model is also improved (see [4,5]) by introducing another optimization technique valid in both electropositive and electronegative gases. This is based on the following considerations. Processes of particle creation (i.e. ionization and detachment) can increase the number of pseudo-particles and, therefore, the computing time. Processes of disappearance (attachment, recombination or loss towards walls) can decrease the accuracy of the result. In order to maintain approximately the same number of simulated particles allowing both a short computing time along with good result accuracy, a new pseudo-particle technique (see [15]) is used. This consists of increasing or decreasing the size of the pseudo-particles by predetermined amounts, when particle creation or disappearance occurs. Another optimization technique is also used. This consists of starting the calculations, not from arbitrary initial conditions but from final conditions already obtained in a previous simulation. Obviously, the use of these optimization techniques leads to results in agreement with the classical PIC/MCC ones but the computing time is reduced by a factor of about 10 in the present RF discharge simulations.

Under the present operating conditions, sustaining the discharge is mainly controlled by the attachment–detachment processes. In our particle model, the associated basic data for electron–N_2O interactions and the main ions (N_2O^+, O^- and NO^-) interacting with N_2O gas have also been detailed elsewhere [4].

The electric and energetic parameters thus obtained are, between others, the spatio-temporal evolution (between the inter-electrode gap during a RF cycle) of the electron and ion densities, the reaction rates, the mean electron and ion energies, the potential, the electric field and the associated dissipated power density.

3.2. Basic data

The basic data needed for our discharge model are the collision cross sections for the different charged particles interacting with the neutral gas. In the case of a N_2O discharge, the main (most abundant) ions are N_2O^+, O^- and NO^- issued from e–N_2O collisions [5]. This means that the present particle model needs prior knowledge of the cross section sets of various systems of charged particles interacting with the gas. The first system is the electron–gas interactions, i.e. e–N_2O, and the second one consists of the ion–gas interactions, i.e. O^-/N_2O, NO^-/N_2O and N_2O^+/N_2O. These different interactions are listed in table 1 with the corresponding references for the collision cross sections.

In fact, the collisions between the electrons and the gas particles lead to the creation of many ions of which we only retained those responsible for discharge sustaining.

These ions, in their turn, undergo collisions with the gas and also lead to the creation of new ions and again we only kept those that have a non-negligible weight on the discharge maintenance (i.e. N_2O^+, O^- and NO^-).

Most of the collision cross sections considered in this work are quite well known even though it had been necessary to solve some problems related to the lack of proper knowledge concerning electron attachment cross section [16].

However, the ion–neutral case is much more problematic because the collision cross sections for the main ions formed by electron impacts on N_2O and interacting with it are not well known. Therefore, a specific method [17] has been

used to obtain the missing collision cross sections in our different ion–neutral systems involved in the N_2O discharge. This concerns more particularly the elastic momentum transfer one in the energy range of our interest in RF discharge reactors (i.e. from thermal energy up to about 100 eV). This also concerns certain inelastic collision cross sections, mainly the charge transfer ones which are measured only in a very limited energy range, and in a less degree the other inelastic processes (electron detachment or ion conversion). In the case of the elastic collision, we used a $(n-4)$ core model for the interaction potential well adapted for the polyatomic systems (see [18, 19]). This allows us to determine the momentum transfer cross sections of the present ion–gas systems using a semi-classical approach based on JWKB approximation (see, e.g. [20]). These elastic collision cross sections are then completed with the inelastic ones which are taken from a literature compilation. In certain cases, due to their lack in the energy range of our interest, these inelastic collision cross sections are completed using the appropriate empirical formalism, as for example Firsov expression for the resonant charge transfer (see, e.g. [19]). The chosen set of collision cross sections is then fitted and validated using a classical swarm unfolding technique (see, e.g. [21]). This means that the chosen collision cross sections are used in an optimized Monte Carlo method [21] for ion swarm data calculations. This allows the validation step from a comparison between the calculated swarm data and the available measured one until the best agreement is obtained.

3.3. Microscopic approach for dissipated power calculation

Generally, the total dissipated power density is deduced from the classical relation including current density $\vec{J}$ and electric field $\vec{E}$ (see [13]) integrated over the space r and time t (T being the RF period):

$$P_{\mathrm{CL}} = \frac{1}{T}\iint \vec{J}\cdot\vec{E}\,\mathrm{d}r\,\mathrm{d}t. \tag{1}$$

As emphasized previously, relation (1) is a macroscopic approach which gives global information about the dissipated power but does not give any information on how this power is dissipated through the different collision processes occurring either in the sheath or in the plasma region. This is why a specific approach is proposed and integrated in the particle discharge model for the calculation of both total and partial power density impossible to obtain with the above classical method and very useful in the analysis of the power density behaviours.

As the power under the present work operating conditions is mainly dissipated by the electron processes (see [4, 5]), the starting point of this specific approach is the usual electron energy conservation equation corresponding to the second moment of Boltzmann equation. It can be written in the following form (see [28])

$$\frac{\partial W_{\mathrm{e}}}{\partial t} + \frac{5}{3}\frac{\partial W_{\mathrm{e}}\cdot\langle\vec{v}_{\mathrm{e}}\rangle}{\partial\vec{r}} - \vec{J}\cdot\vec{E} = -n_{\mathrm{e}}\sum_j \varepsilon_{\mathrm{ex},j}\langle\nu_{\mathrm{ex},j}\rangle$$
$$-n_{\mathrm{e}}\varepsilon_{\mathrm{ion}}\langle\nu_{\mathrm{ion}}\rangle - n_{\mathrm{e}}\langle\varepsilon_{\mathrm{e}}\nu_{\mathrm{at}}\rangle - n_{\mathrm{e}}\frac{2m_{\mathrm{e}}}{M}\langle\varepsilon_{\mathrm{e}}\nu_{\mathrm{el}}\rangle, \tag{2}$$

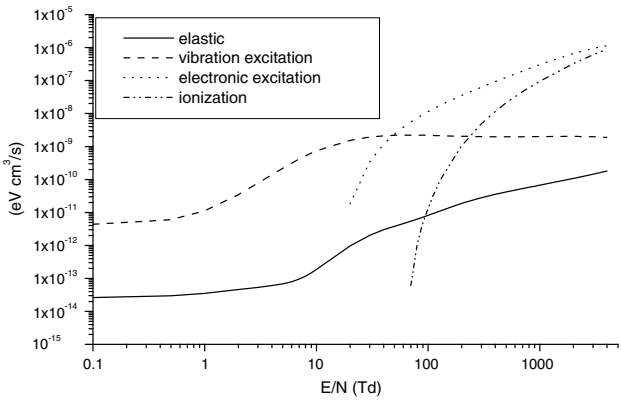

Figure 3. Source terms of energy equation (2) for, respectively, elastic collision, vibration excitation, electronic excitation and ionization, as a function of the reduced dc-electric field E/N.

where $W_{\mathrm{e}}(\vec{r},t)$ is the energy density (i.e. $n_{\mathrm{e}}\cdot\langle\varepsilon_{\mathrm{e}}\rangle$), n_{e} the electron density, ε_{e} the energy of the electron and $\langle\vec{v}_{\mathrm{e}}\rangle$ its average velocity. $n_{\mathrm{e}}\sum_j \varepsilon_{\mathrm{ex},j}\langle\nu_{\mathrm{ex},j}\rangle$ represents the energy source term relative to the excitation processes of different j levels, whereas $n_{\mathrm{e}}\varepsilon_{\mathrm{ion}}\langle\nu_{\mathrm{ion}}\rangle$ and $n_{\mathrm{e}}\langle\varepsilon_{\mathrm{e}}\nu_{\mathrm{at}}\rangle$ are, respectively, the ionization and the attachment energy source terms. Terms between brackets correspond to the quantity averaged over the distribution function $f(\vec{v}_{\mathrm{e}},\vec{r},t)$ in the velocity space. For example, the ionization frequency $\langle\nu_{\mathrm{ion}}\rangle$ is defined as $n_{\mathrm{e}}(\vec{r},t)\langle\nu_{\mathrm{ion}}\rangle = \iiint_{\vec{v}_{\mathrm{e}}} f(\vec{v}_{\mathrm{e}},\vec{r},t)\nu_{\mathrm{ion}}\mathrm{d}\overrightarrow{v_{\mathrm{e}}}$ (ν_{ion} is a microscopic collision frequency).

As for ν_{ion}, the quantities ν_{at}, ν_{ex} and ν_{el} are, respectively, the attachment, excitation and elastic frequency.

The product $\vec{J}\cdot\vec{E}$ used in the macroscopic definition of the power density dissipation (see equation (1)) is directly obtained from equation (2):

$$\vec{J}\cdot\vec{E} = n_{\mathrm{e}}\sum_j \varepsilon_{\mathrm{ex},j}\langle\nu_{\mathrm{ex},j}\rangle + n_{\mathrm{e}}\varepsilon_{\mathrm{ion}}\langle\nu_{\mathrm{ion}}\rangle + n_{\mathrm{e}}\langle\varepsilon_{\mathrm{e}}\nu_{\mathrm{at}}\rangle$$
$$+ n_{\mathrm{e}}\frac{2m_{\mathrm{e}}}{M}\langle\varepsilon_{\mathrm{e}}\nu_{\mathrm{el}}\rangle + \frac{\partial W_{\mathrm{e}}}{\partial t} + \frac{5}{3}\frac{\partial W_{\mathrm{e}}\cdot\langle\vec{v}_{\mathrm{e}}\rangle}{\partial\vec{r}}. \tag{3}$$

The integration of expression (3) during a RF cycle (in the time interval $[0,T]$) directly gives the following relation (4) pertaining to the steady state and for a negligible energy exchange term for elastic collisions in comparison with inelastic collisions:

$$P = \frac{1}{T}\iint \vec{J}\cdot\vec{E}\,\mathrm{d}r\,\mathrm{d}t = \frac{1}{T}\iint \mathrm{d}r\,\mathrm{d}t\left(n_{\mathrm{e}}\sum_j \varepsilon_{\mathrm{ex},j}\langle\nu_{\mathrm{ex},j}\rangle\right.$$
$$\left. + n_{\mathrm{e}}\varepsilon_{\mathrm{ion}}\langle\nu_{\mathrm{ion}}\rangle + n_{\mathrm{e}}\langle\varepsilon_{\mathrm{e}}\nu_{\mathrm{at}}\rangle + \frac{5}{3}\frac{\partial W_{\mathrm{e}}\cdot\langle\vec{v}_{\mathrm{e}}\rangle}{\partial\vec{r}}\right). \tag{4}$$

Indeed, shown in figure 3 are the different source terms of energy equation (2) as a function of the reduced electric field E/N: $(2m_{\mathrm{e}}/M)(\langle\varepsilon_{\mathrm{e}}\nu_{\mathrm{el}}>/N)$ for elastic collision, $\sum_{\mathrm{vib}}\varepsilon_{\mathrm{ex,vib}}(\langle\nu_{\mathrm{ex,vib}}\rangle/N)$ for vibration excitation, $\sum_{\mathrm{elec}}\varepsilon_{\mathrm{ex,elec}}(\langle\nu_{\mathrm{ex,elec}}\rangle/N)$ for electronic excitation and $\varepsilon_{\mathrm{ion}}(\langle\nu_{\mathrm{ion}}\rangle/N)$ for ionization. It is easy to observe in this figure that the elastic term corresponding to the energy exchange during elastic collision is much lower than the other terms (excitation or ionization), which therefore justifies its omission in relation (4).

In fact, such an observation had been mentioned by Holstein [29] in a paper devoted to the elaboration of an equation for the energy distribution of electrons in a weakly ionized gas subject to high frequency fields. Moreover, in their study of paired rings in pulsed capacitive RF discharges, Sakawa and Shoji [30] also found that energy loss by elastic collisions was very small.

Other authors (see, for example [31, 32]) also found that elastic collisions could be neglected in weakly ionized low pressure discharges.

From an appropriate sampling technique used in the present Monte Carlo technique for the collision treatment, it becomes easy to calculate separately the terms of attachment, ionization and excitation (both for vibration and electronic levels).

The sum of these collision terms corresponds in fact, before their integration, to the deposited energy density in gas by electron impacts. The sampling relation used to estimate the deposited energy density can be written as a function of either time W^k or position W_i:

$$W^k = \sum_i W^k_{\mathrm{ex},i} + \sum_i W^k_{\mathrm{ion},i} + \sum_i W^k_{\mathrm{at},i} \quad \text{or}$$

$$W_i = \sum_k W^k_{\mathrm{ex},i} + \sum_i W^k_{\mathrm{ion},i} + \sum_i W^k_{\mathrm{at},i}, \tag{5}$$

where index i and k of the energy density corresponds, respectively, to the discretization of space z belonging to domain $[0, z_{\max}]$ and time t belonging to domain $[0, T]$:

$$[0, z_{\max}] = [z_0 = 0, z_1, \ldots, z_{i-1}, z_i, z_{i+1}, \ldots, z_I = z_{\max}],$$

$$[0, T] = [t_0 = 0, t_1, \ldots, t_{k-1}, t_k, t_{k+1}, \ldots, t_I = T].$$

Once the different deposited energy terms (W^k_{ex}, W^k_{ion} and W^k_{at}) are calculated from the Monte Carlo treatment of the collisions, the dissipated power density P^k can be simply deduced from the energy deposition term W^k corresponding to the sum of the different process contributions divided by the time:

$$P^k = \frac{W^{k+1} - W^k}{\Delta t} \tag{6}$$

with $W^k = W^k_{\mathrm{ex}} + W^k_{\mathrm{ion}} + W^k_{\mathrm{at}}$.

Then the average discrete sum of expression (6) over a RF time cycle T leads directly to the dissipated power density (P_{MC}) which can be compared with the classical expression P_{CL} given in relation (1). As shown in expression (4), the possible differences between P_{CL} and P_{MC} can come from the heat current flow term (i.e. $\frac{5}{3}(\partial W_{\mathrm{e}} \cdot \langle \vec{v}_{\mathrm{e}} \rangle / \partial \vec{r})$) which is calculated in section 4 devoted to results.

4. Results and discussion

4.1. Particle model results and collision processes' contribution to power dissipation

The experimental evolutions of the total power density as a function of the applied voltage are presented in figure 4 as well as the total power densities calculated using the classical method and the microscopic approach at a gas temperature of 503 K and gas pressures of 0.5 and 1 Torr. The total dissipated powers calculated by the two methods are very close to each other. This can be easily explained based on equation (4), where it is obvious that the difference between the two approaches originates from the heat current term ($\frac{5}{3}(\partial W_{\mathrm{e}} \cdot \langle \vec{v}_{\mathrm{e}} \rangle / \partial \vec{r})$), which is in fact negligible under the present working conditions. For example, under 100 V and 1 Torr, while the total dissipated power density is 11.5 mW cm^{-2}, the corresponding value of the heat current term is 7.6×10^{-5} mW cm^{-2}.

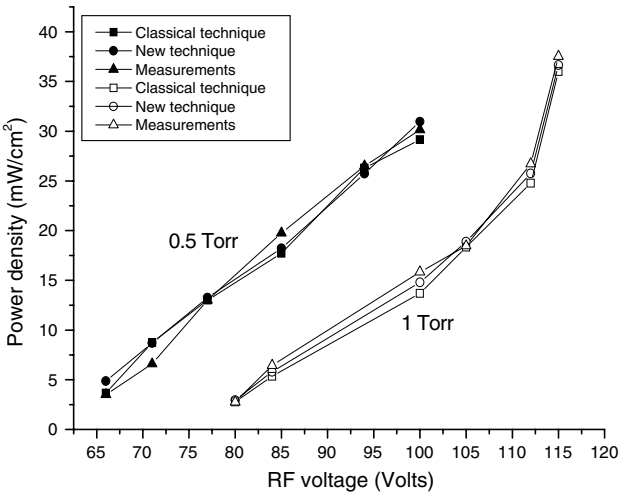

Figure 4. Power density as a function of RF voltage at 0.5 and 1 Torr: comparison between the two calculation techniques and the experimental results.

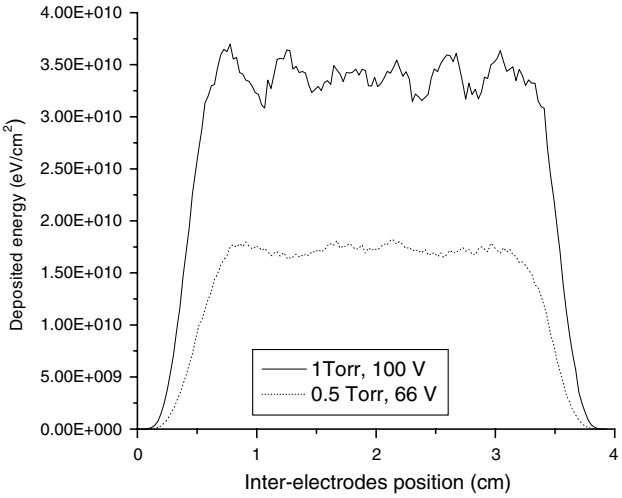

Figure 5. Density of energy as a function of the inter-electrode distance, at 0.5 Torr and 66 V for RF voltage.

Using the present approach of the power density calculation, the total powers (e.g. those of figure 4) are then obtained. In addition, from the present approach, it is also possible to obtain the variation of both the time-averaged and the space-averaged dissipated energy. These quantities are, respectively, presented in figure 5 (1 T, 100 V and 0.5 T, 66 V) as a function of the position in the space gap, and figure 6 (1 T, 100 V and 0.5 T, 66 V) as a function of the RF cycle. Figures 5 and 6, typical of RF discharges in electronegative gases (see table 2 for electronegativity in some cases), clearly show that the energy and consequently the power, having a sinusoidal variation as a function of time, are essentially dissipated in

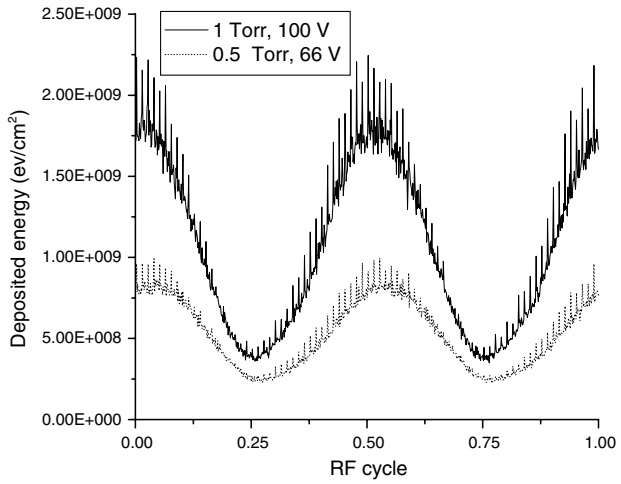

Figure 6. Energy density evolution as a function of a RF cycle at 0.5 Torr and 66 V RF voltage.

Table 2. Some electronegativity calculated at the bulk plasma for three cases of the studied N_2O discharge.

Working conditions	Electronegativity (N_n/N_p)
66 V, 0.5 Torr	0.846
100 V, 1 Torr	0.797
112 V, 1 Torr	0.712

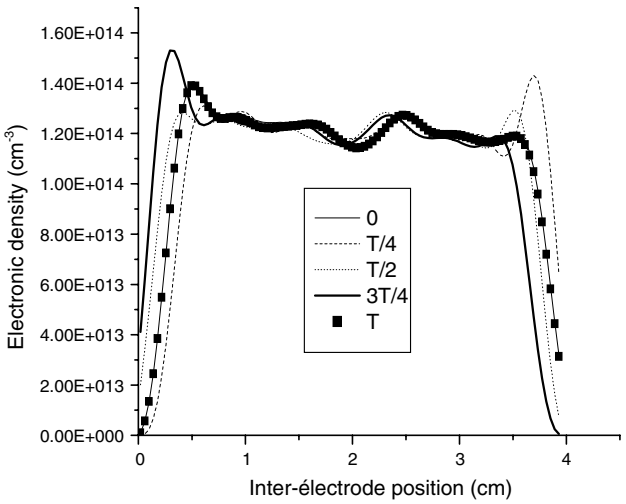

Figure 7. Electronic density evolution as a function of inter-electrode position at different instants of the RF cycle, at 1 Torr and 100 V.

the positive column, which was observed under our working conditions at 0.5 as well as 1 Torr. This result is due to the fact that energy is mostly dissipated by electrons whose density reaches its maximum in the space gap where it is practically constant, as shown in figure 7.

The spatial and the time profile of the deposited energy or the power density can also be obtained from the classical technique. The power density calculations (see figure 4) using the classical or the microscopic technique are very close, and thus the spatial and the time profiles of the dissipated power by the two techniques are also similar.

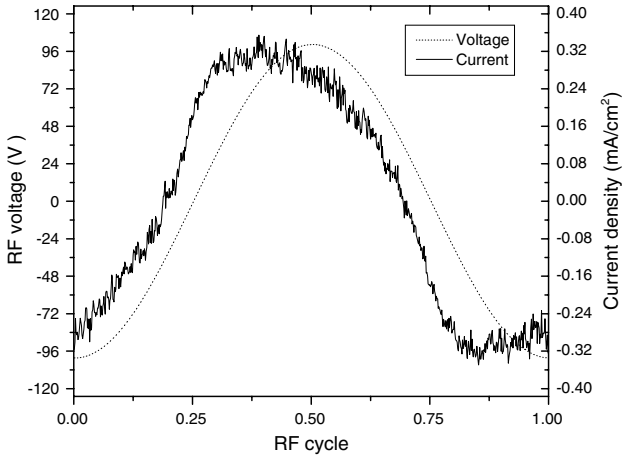

Figure 8. RF voltage and discharge current density during a RF cycle.

In addition, in order to understand the temporal behaviour of the dissipated power density, a voltage–current characteristic, $V(t)$ (RF voltage) and $J(t)$ (discharge current density), for a pressure of 1 Torr and a voltage of 100 V, during a period (a RF cycle), is shown in figure 8. The phase shift between the current and the voltage is approximately equal to $\pi/6$.

This information permits to deduce the average bulk plasma resistance and sheaths capacity.

Furthermore, up to now, there were no direct means to elucidate the collision processes responsible for the power dissipation, but to infer them based on indirect results such as the electron density and their mean energy. The direct acquisition of the three different terms corresponding to the electron energy deposition by excitation, ionization and attachment processes (see equation (5)) renders the power dissipation interpretations almost straightforward permitting to analyse the power density behaviour by studying the balance between the ionization and attachment processes as we will see hereafter.

Figure 9 is a typical illustration of what can be obtained with our specific microscopic approach. The relative contribution of the excitation, attachment and ionization processes to the total power are given as a function of the RF applied voltage at 0.5 and 1 Torr. The first feature of these results is that, at a given voltage, the main power deposition process is incontestably the excitation whose contribution is around 90%, which is coherent with our working conditions corresponding to cold plasma discharges. The role of this process is not discussed often enough in discharge analyses since it does not contribute to sustain the discharge either by electron loss or production. In fact, due to the high number of the low energetic electrons in our discharge and the low value of the excitation threshold of vibration levels (i.e. 0.069, 0.15 and 0.26 eV for v2, v3 and v1 vibration modes), the excitation definitely appears as the main source for power dissipation. The former explanation also allows understanding why the excitation contribution percentage decreases either as the applied voltage increases or as the pressure decreases. Both variations result in a relative increase in the higher energetic electrons to the detriment of the low energetic ones

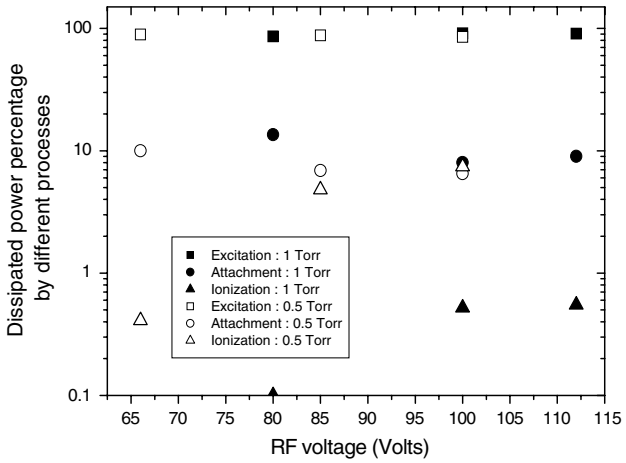

Figure 9. Percentage of contribution of each inelastic process to the total power dissipation for different RF voltages, at 0.5 and 1 Torr.

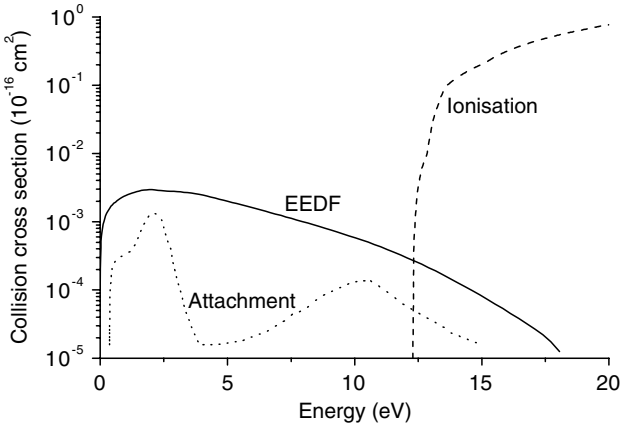

Figure 10. Energy distribution function EEDF (in arbitrary units) for a 2.8 eV electron mean energy (——) with attachment and ionization collision cross sections (· · · · · · and - - - -).

and therefore to the aforementioned excitation contribution decrease.

If the power density module is mainly controlled by the excitation process, the variation of this power density is principally due to the attachment and ionization processes. It is then very interesting to analyse these two non-conservative processes (attachment and ionization) which, respectively, have a threshold of 0.36 eV and 12.3 eV.

In figure 9, the decrease in the attachment contribution is much smoother than the increase in the ionization process. This is very coherent with our working conditions being typical of cold plasma processing.

Indeed, under these conditions, even if some electrons reach the energy level to be able to ionize (noting, however, that these electrons are directly responsible of such an increase in the ionization contribution, as we will see below), the large majority of electrons have rather low energy, typically around 2.3 eV (see figure 10 showing the electron energy distribution function EEDF, attachment and ionization cross sections). This always leads to a large amount of electrons with the ability to attach (noting, however, that these electrons are directly responsible for the smooth increase in the attachment contribution, as we will see below). The large increase in the ionization contribution, which almost corresponds to two decades at 0.5 Torr when the applied voltage varies from 66 to 100 V, is a direct consequence of the high value of the ionization threshold and correlates with the rise of the higher energy distribution tail of the electron energy distribution. At 0.5 T and 100 V, one can remark that the ionization contribution even goes beyond that of the attachment. This might be surprising considering that the attachment threshold is much lower than that of ionization. In fact, this inversion is probably a result of the particular shape of the attachment cross section (see figure 10) which rapidly decreases after reaching its maximum at which position the energy is around 2 eV.

It is not that the ionization energy exceeding means inevitably that the ionization rate is more important than that of the attachment even at 0.5 T and 100 V; the average energy relates to the low energy domain and the attachment rate is much greater than that of ionization, as we can see in figures 12 and 13 in the following section. For example, at 0.5 T and 100 V, the attachment rate is approximately 25 times the ionization rate.

Moreover, for a better understanding of the term exceeding, it is sufficient to remark that the mean free path at 0.5 Torr is more important than the one at 1 Torr, which as a consequence, increases the electron mean energy favouring the ionization. It should also be remarked that the ionization threshold energy is approximately 50 times that of attachment. In other words, only one ionization is equivalent, from the deposited energy point of view, to 50 attachments. Thus, in terms of dissipated power, we can easily understand, provided the working conditions, that the ionization process can have a more important weight than the attachment process in the power dissipation (like the case of 0.5 T and 100 V), without the necessity of a very high number of ionizations as regards the number of attachments.

4.2. Power dissipation

Let us now study the evolution of the power density as a function of the RF voltage at 0.5 and 1 Torr.

4.2.1. An unexpected variation of the power density at the pressure of 1 Torr. One can remark in figure 4 above that at 0.5 Torr, the power density grows linearly whereas at 1 Torr it starts by growing linearly until a voltage of the order of 110 V beyond which it presents a steeper gradient. This change behaviour can be explained, with the help of our particle model, in terms of creation and loss of electrons given that the variation of the power density is essentially controlled by the electron density variation, which is proportional to the power variation, as shown in figure 11. This leads us to examine the processes which are responsible for the creation (i.e. ionization and detachment) and loss (i.e. attachment) of electrons. To this end, we will study the reaction rate variation of each of the three processes.

Note that the competition between these processes (attachment, detachment and ionization) was first discussed in O_2RF plasma by Shibata *et al* [33], with a special emphasis on the plasma density and the number densities of $O_2(a\,^1\Delta_g)$ and atomic oxygen for the different voltages and pressures they considered.

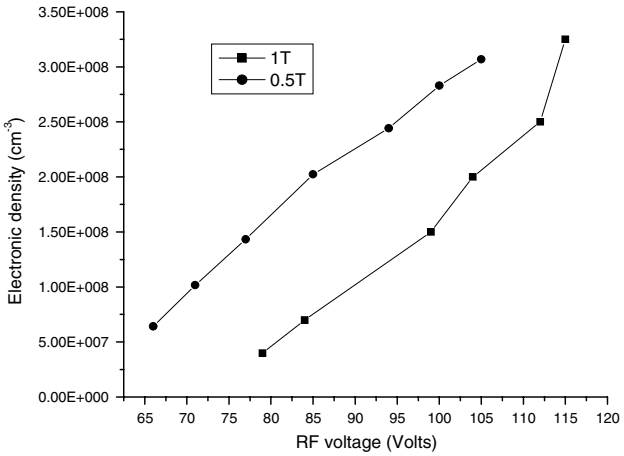

Figure 11. Electronic density as a function of RF voltage at 0.5 and 1 Torr.

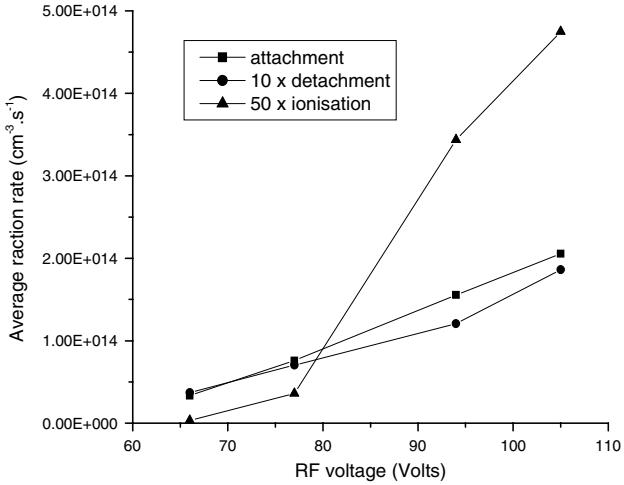

Figure 12. Reaction rates of the attachment, detachment and ionization processes as a function of RF voltage, at a pressure of 0.5 Torr.

These reaction rates are obtained by multiplying the reaction constant of a process by the density of the treated charged particle and the gas density, once the stationary equation (including terms of flows which represent the gains and losses of mobility and diffusion) is checked and respected, after the steady state is reached in the discharge.

Note that the evolution of the reaction rates can explain the evolution of the power density as a function of RF voltage, but the power magnitude is mainly controlled by the excitation processes at a given pressure and RF voltage, as already shown in the preceding section.

4.2.2. Analysis of the power variation. By examining figure 12, we can see that at 0.5 Torr, the power density linear growth is principally due to the linear growth of the ionization rate; the attachment and detachment rates varying in the same way. At 1 Torr (figure 13) we can distinguish two regimes according to voltage being higher or lower than about 110 V.

For voltages below than 110 V, the linear power variation is partly due to the linear variation of the ionization but more particularly to the quasi-constant detachment gradient which

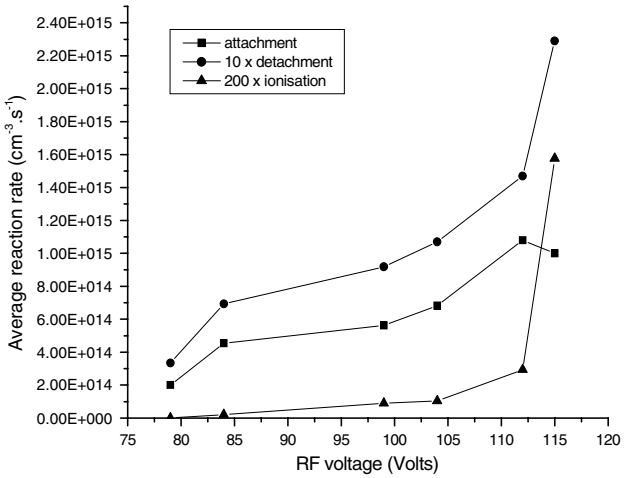

Figure 13. Reaction rates of the attachment, detachment and ionization processes as a function of RF voltage, at a pressure of 1 Torr.

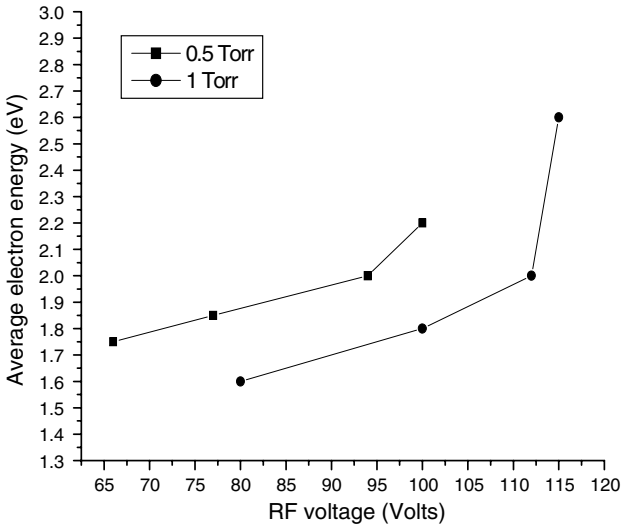

Figure 14. Average electron energy as a function of RF voltage, at 0.5 and 1 Torr.

is slightly superior to the attachment one but sufficient to make the power grow constantly. For voltages higher than 110 V, the power is controlled by the three processes acting together in a way that makes the power increase suddenly.

Concretely, the attachment begins to decrease because the attachment coefficient shows a maximum [5] for an electron energy that corresponds to the mean electron energy in our discharge at 110 V. Furthermore, by considering the region of the attachment cross section that corresponds to the energy area of our interest, one can easily see in figure 10 above, that this cross section presents a maximum for an energy around 2 eV.

On the other hand, the ionization gradient becomes more important because the electrons are now more energetic at these relatively high voltages, as we can see in figure 14 representing the average electron energy as a function of the RF voltage.

Moreover, the detachment gradient also becomes relatively important in spite of an attachment decrease which leads to less O^- formation. In fact, the NO^- ionic conversion (i.e. $O^- + N_2O \rightarrow NO^- + NO$) cross section is relatively more

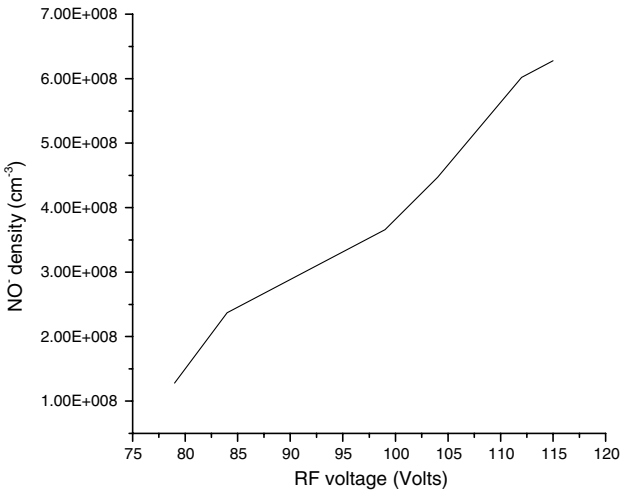

Figure 15. NO^- density as a function of RF voltage at a pressure of 1 Torr.

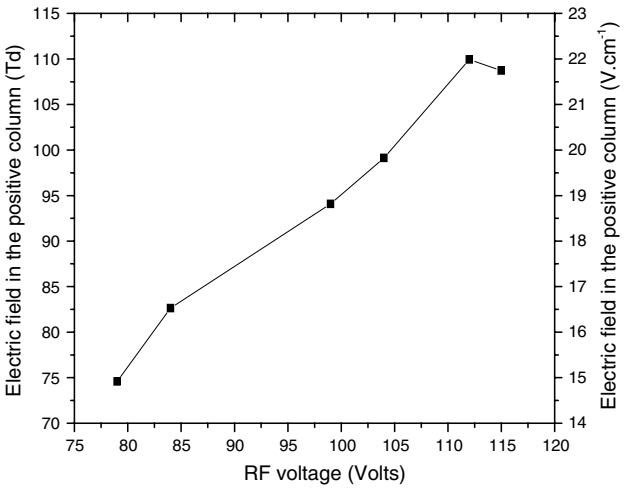

Figure 16. Electric field in the positive column as a function of RF voltage at a pressure of 1 Torr.

important for the voltages under consideration and leads to an increase in the NO^- density (see figure 15) and consequently to an increase in the detachment process (i.e. $NO^- + N_2O \rightarrow NO + N_2O + e$), leading, of course, to an increase in the detachment rate and so contribute to an increase in the electron density, provided that the detachment cross section is quasi-constant over the energy levels of our interest (less than 0.1 eV for all ions). Thus, the sudden power density increase starting from a voltage around 110 V can be explained by the sudden increase in the electron density due to an attachment decrease and ionization and detachment increase.

Note that in the latter case, when the voltage increases from 110 V, the electric field increase is important in the sheaths while it decreases in the positive column (see figure 16). This has a double consequence: an increase in ionization coming from electrons accelerated in the sheaths and a decrease in attachment (electrons becoming more energetic). This increase in external electrons leads to a decrease in the electric field in the positive column, and then to a diminution of the O^- energy favourable to the ionic conversion process. The NO^- production is thus found to increase. This latter aspect is favourable to an augmentation in the detachment rate favouring

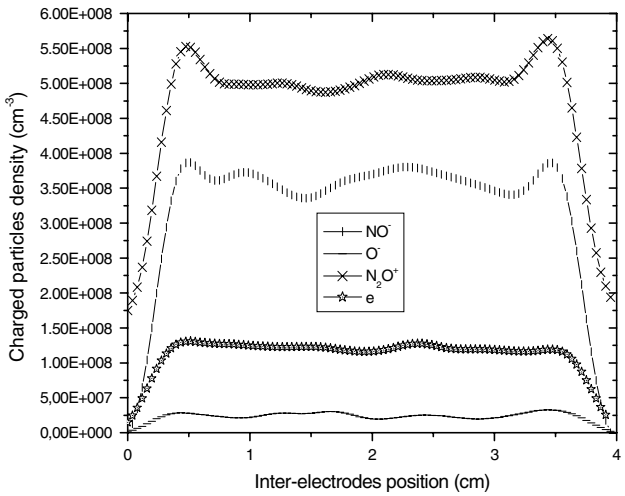

Figure 17. Density of different charged particles as a function of position for a pressure of 1 Torr and a voltage of 100 V.

the presence of electrons in the positive column to the detriment of negative ions, leading to a decrease in the electronegativity as we can see in table 2. This electronegativity at the bulk plasma (positive column) is calculated by dividing the density of negative ions (i.e. NO^- and O^-) by the density of positive ions (i.e. N_2O^+), which are quasi-constants in the positive column as shown in figure 17 for a pressure of 1 Torr and a voltage of 100 V.

5. Conclusion

The microscopic approach, in the framework of a particle modelling, presented in this paper for the partial and total dissipated power in a cold low pressure N_2O RF discharge, is a very interesting and straightforward tool to understand how the electrical power is converted in the discharge, and especially to analyse the energy deposition by the different collision processes. It was shown that the main power dissipation sources were the excitation processes for given experimental conditions of voltage and pressure, while the variation of the power dissipation as a function of applied voltage was principally due to the contribution of attachment, detachment and ionization processes. So far as these latter processes are concerned, their relative contribution depends highly on the distribution of the electron energy: the higher their energy (lower pressure, higher voltage), the higher the impact of the ionization, especially due to the particular shape of the attachment cross section.

It has been shown that at 0.5 Torr, the linear growth of the power density is principally due to the linear growth of the ionization rate, while we can distinguish two different regimes at 1 Torr separated by a voltage around 110 V. At voltages lower than 110 V, the linear power variation is mainly due to the linear variation of the detachment gradient. At voltages higher than 110 V, the sudden power increase is due to a rapid increase in the ionization and detachment rates together with an attachment decline.

The role played by the electrons and the negative ions in the discharge sustaining has then been analysed showing the influence of the electronic and negative ion energy on the electron, O^- and NO^- production.

We also showed that the power density calculated with the help of our microscopic approach was very close to the one calculated with the classical macroscopic relation, showing then that a heat current flow could be neglected in the cold low pressure N_2O RF discharges. The good agreement between the theoretical calculations and the power density measurements permits validation of our particle model for energy calculations along with the processes considered with their cross sections. A complete database was then elaborated and validated in order to characterize N_2O low pressure cold discharges. This will be of great help for our future studies which will concern the modelling of N_2O/SiH_4 mixtures used to deposit silicon oxide thin films.

Finally, it seems important to note that when the data base (processes and cross sections) of any collisional system for a given discharge is already established, the application of this microscopic technique with a Monte Carlo code is a powerful method permitting a fully and detailed electric and energetic characterization of the discharge.

References

[1] Liberman M A and Lichtenberg A J 1994 *Principles of Plasma discharges and Materials Processing* (New York: Wiley)
Kushner M J 1993 *J. Appl. Phys.* **74** 6538
Lisovsky V A 1995 *IEEE Int. Conf. on Plasma Science (New York)* p 145

[2] Adams A C, Alexander F B, Capio C D and Smith T E 1981 *J. Electrochem. Soc.* **128** 1545
Eagle D J and Milne W I 1987 *Thin Solid Films* **147** 259
Gokan H, Morimoto A and Murahata M 1987 *Thin Solid Films* **149** 85

[3] Green M L, Gusev E P, Degraeve R and Garfunkel M L 2001 *J. Appl. Phys.* **90** 2057
Batey J and Tierney E 1986 *J. Appl. Phys.* **60** 3136
Ambrée P, Wandel K, Böttcher E H and Bimberg D 1995 *J. Appl. Phys.* **77** 945

[4] Daté L, Radouane K, Despax B, Yousfi M, Caquineau H and Hennad A 1999 *J. Phys. D: Appl. Phys.* **32** 1478

[5] Radouane K, Daté L, Yousfi M, Despax B and Caquineau H 2000 *J. Phys. D: Appl. Phys.* **33** 1332

[6] Roldán A Pérez J M, Williart A, Blanco F and García G 2004 *J. Appl. Phys.* **95** 5865

[7] Leger J, Yousfi M, Eichwald O, Loiseau J F and Held B 2004 *15th Int. Conf. on Gas Discharges and their Applications (Toulouse)* p 953

[8] Franke St, Deutsch H, Dinklage A, Solyman S and Wilke C 2001 *J. Phys. D: Appl. Phys.* **34** 340

[9] Hagelaar G J M, Klein M H, Snijkers R J M M and Kroesen G M W 2001 *J. Appl. Phys.* **89** 2033

[10] Koo J W and Boyd I D 2003 *39th AIAA/ASME/SAE/ASEE Joint Propulsion Conf. (Huntsville)* p 10133

[11] Dimitris P Lymberopoulos and Demetre J Economou 1995 *J. Res. Natl. Inst. Stand. Technol.* **100** 473

[12] Kawamura E and Ingold J H 2001 *J. Phys. D: Appl. Phys.* **34** 3150

[13] Paranjpe A P, McVittie J P and Self S A 1990 *Phys. Rev.* A **41** 6949
Cherrington B E 1979 *Gaseous Electronics and Gas Lasers* (New York: Pergamon)
Roberto M, Smith H B and Verboncoeur J P 2003 *IEEE Trans. Plasma Science* **31** 1292

[14] Godyak V A and Piejak R B 1990 *J. Vac. Sci. Technol.* A **8** 3833
Howling A A, Hollenstein C, Paris P J, Fuger F and Kroll G 1991 *20th Int. Conf. on Plasma Ionized Gases (Pisa)* ed V Palleschi and M Vaselli (Pisa: Instituto di Fisica) **5** p 1089

[15] Sommerer T J and Kushner M J 1992 *J. Appl. Phys.* **71** 1654

[16] Younis G 2005 *PhD Thesis* Paul Sabatier University, Toulouse

[17] Yousfi M and Benabdessadok M D 1996 *J. Appl. Phys.* **80** 6619

[18] Mason E A, O'Hara H and Smith F J 1972 *J. Phys.* B **5** 169

[19] Nelson D, Benhenni M, Eichwald O and Yousfi M 2003 *J. Appl. Phys.* **94** 96
Nelson D, Benhenni M, Yousfi M and Eichwald O 2001 *J. Phys. D: Appl. Phys.* **34** 3247
Benhenni M, Urquijo J, Yousfi M, Hernandez-Avila J L, Merbahi N, Hinojosa G and Eichwald O 2005 *Phys. Rev.* E **71** 036405

[20] Jeffreys H 1925 *Proc. Lond. Math. Soc.* **23** 428
Munn R J, Mason E A and Smith F J 1964 *J. Chem. Phys.* **41** 3978

[21] Yousfi M, Hennad A and Eichwald O 1998 *J. Appl. Phys.* **84** 107
Hennad A 1996 *PhD thesis* Paul Sabatier University, Toulouse
Nelson D 2002 *PhD thesis* Paul Sabatier University, Toulouse

[22] Hayashi M and Niwa N 1987 *Electron collision cross sections for C_2F_6 and N_2O, Gaseous Dielectrics V* ed L G Christophorou and W Bouldin (New York: Pergamon) p 27

[23] Freund R S and Klemperer W 1967 *J. Chem. Phys.* **47** 2897

[24] LeClair L R and McConkey J W 1993 *J. Chem. Phys.* **99** 4566

[25] Dutton J, Gallagher J W, Beaty E C and Pitchford L C 1982 *A Compilation of Electron Swarm Data in Electronegative Gases (22)* p 203

[26] Rapp D and Englander-Golden P 1965 *J. Chem. Phys.* **43** 1464

[27] Paulson J F 1970 *J. Chem. Phys.* **52** 959

[28] Kanzari Z, Yousfi M and Hamani A 1998 *J. Appl. Phys.* **84** 4161

[29] Holstein T 1946 *Phys. Rev.* **70** 367

[30] Sakawa Y and Shoji T 2001 *Plasma Phys.* **8** 2998

[31] Seo S H, Chung C W, Hong J I and Chang H Y 2000 *Phys. Rev.* E **62** 7155

[32] Kolobov V I and Hitchon W N G 1995 *Phys. Rev.* E **52** 972

[33] Shibata M, Nakano N and Makabe T 1996 *J. Appl. Phys.* **80** 6142